JOURNAL OF CATALYSIS 113, 267–280 (1988)

The Design and Preparation of Planar Models of Oxidation Catalysts

I. Hopcalite

CHEONHO YOON AND DAVID L. COCKE

Department of Chemistry, Texas A&M University, College Station, Texas 77843

Received February 2, 1987; revised April 11, 1988

At present there exists a need for methods for the preparation of planar models of a variety of heterogeneous catalysts. The preparation of planar models of oxidation catalysts that contain two or more cations represents a considerable challenge. In this paper we report the preparation of a planar model of the very active deep oxidation catalyst, Hopcalite ($CuMn_2O_4$), by alloy oxidation. This mixed valent oxide was obtained only after detailed study of the effects of oxidation temperature, oxygen activity, and Cu–Mn alloy composition on the structure and chemistry of the oxide overlayer. In most cases layered structures of Mn oxides and Cu oxides were obtained. Only under a very specific set of conditions could the mixed valent oxide be prepared. The oxidation processes were monitored by X-ray photoelectron spectroscopy (XPS) and from this the structure and chemistry of the overlayers were determined. Hopcalite was identified at the surface by comparison of the XPS spectra with those of a commercial sample and the presence of an unusually low-binding-energy Cu($2p$) line in the crystalline $CuMn_2O_4$ state. The preliminary catalytic activity of the planar model catalyst is compared with that of the commercial catalyst. © 1988 Academic Press, Inc.

INTRODUCTION

One purpose of basic scientific studies of catalytic systems is to understand how they work on an atomic scale. One aims to identify the active sites where bond breaking and rearrangement take place and to detect surface intermediates formed during the reaction. Studies have been conducted to determine how the atomic surface structure and surface composition influence catalytic activity and selectivity. However, working catalyst systems have complicated structures that do not lend themselves easily to atomic scale investigations. For example, the internal pore structure of high-surface-area supports hides the metal particles and makes it difficult to determine surface structure, elemental composition, and oxidation states. Conventional high-surface-area catalysts usually require grinding and pressing into disks for characterization by surface science techniques. This can expose the samples to unwanted inner structures and to potential contamination by the grinding process or by the exposure to uncontrolled atmospheres. To overcome this problem, model catalysts are now being developed and studied. For instance, alumina planar model catalysts (*1*) have gained attention as models for working catalysts because of their attractiveness for study by modern surface analytical techniques (*2*), electron optical methods (*3*), and reflection spectroscopy (*4–7*). In this context "planar" means a thin flat oxide layer or free-standing oxide of uniform thickness (<1 μm). Advantages of using the model catalysts are that their surface structure and composition can be prepared with uniformity and characterized by the many available surface diagnostic techniques.

Hopcalite, $CuMn_2O_4$, is a well-known oxidation catalyst (*8–10*). It is used for the removal of air pollutants such as carbon monoxide and nitrous oxide from exhaust gas (*11, 12*). It is also important in respiratory protection in military, mining, and

0021-9517/88 $3.00
Copyright © 1988 by Academic Press, Inc.
All rights of reproduction in any form reserved.

TABLE 1

Materials, Their Compositions, Purities, and Sources

Materials	Purities	Sources
Cu shot	99.9999	Johnson Matthey Inc.
Cu–Mn(10%) disk	99.9	Prepared
Cu–Mn(33%) disk	99.9	Prepared
Cu–Mn(50%) disk	99.9	Prepared
Cu–Mn(67%) disk	99.9	Prepared
Cu–Mn(81%) film	99.772	Reactor Experiments Inc.
Mn flake	99.995	Johnson Matthey Inc.
Hopcalite powder	99.7	Auergesellschaft, Berlin, granule size 1.0–1.5 mm

space applications (*13, 14*). Hopcalite is highly active in an amorphous state even at room temperature and it loses activity at temperatures above ca. 500°C where crystallization to $CuMn_2O_4$ spinels occurs (*15–17*). However, this is a controversial point since crystalline $CuMn_2O_4$ has also been reported by Schwab and Kanungo to be active (*18*). They suggested that electron transfer between two different valence states of both Cu and Mn within the spinel lattice is related to the extremely high oxidation activity. The charge exchange system

$$Mn(III) + Cu(II) = Cu(I) + Mn(IV)$$

has since been discussed by several researchers to explain the abnormal activity of Hopcalite (*17–21*), as well as of other catalysts (*22*). Direct experimental evidence for this redox couple was obtained by Veprek *et al.* through the use of X-ray photoelectron spectroscopy (XPS) (*23*). Unfortunately, because of potassium segregation, which is irreversible and causes catalyst deactivation, it was not possible to tie the redox couple directly to catalytic activity. Therefore, the catalytic importance of the oxidation states in the Hopcalite catalyst must still be determined. The determination of the active sites, the role of the Cu promoter, and the mechanisms of oxidation and deactivation in this catalyst should be explored with a pure Hopcalite system—free of promoters and dopants. This requires a clean, well-defined planar model catalyst.

The object of this study was to prepare a planar model of this highly active oxidation catalyst, Hopcalite, by controlled oxidation of Cu–Mn alloys. Fundamental and preliminary studies on the pure Cu and Mn systems and the more complex Cu–Mn alloys have been reported elsewhere (*24*). In this paper we concentrate on the design and preparation of model Hopcalite catalysts based on the understanding achieved in the above work.

EXPERIMENTAL

The materials studied are given in Table 1. The alloys were produced by an arc melting device from Cu shot and Mn flake. The arc melting device with a water-cooled copper crucible was operated at about 10 Torr argon. The bulk compositions of the alloys were checked by an electron beam microprobe. The alloys were found to be homogeneous after several remelting and turning cycles. Specimens were prepared by abrading with fine sandpaper (600 SiC), followed by polishing with 1-μm diamond paste. Research-grade oxygen from Scientific Gas Products (Ashland Chemical Co.) and sputter-grade argon (99.9999% Ar and <0.5 ppm O_2) from Scott Specialty Gases (Scott Environment Technology, Inc.) were used and manipulated in a separate preparation chamber attached to an X-ray photoelectron spectrometer.

Details of the oxidation behavior of these Cu–Mn alloys can be found in the literature (*24*). Based on these studies, surface mixed oxides were prepared at atmospheric pressure. Specimens were positioned on a glass plate in the center of a cylindrical quartz tube within a furnace. They were treated at 30°C and from 100 to 500°C in intervals of 100°C for 1 h in 1 atm oxygen flowing through the quartz tube at the rate of 30 ml/min. The alloy samples examined were Cu–Mn(10%), Cu–Mn(33%), Cu–Mn(50%), Cu–Mn(67%), each being a 1.5-mm-thick disk, and a Cu–Mn(81%) film. In order to compare surface oxides prepared in this study to a working catalyst, commer-

cial Hopcalite was activated at 220°C for 2 h in 1 atm oxygen flow (ca. 30 ml/min). A commercial sample was also heated at 550°C for 10 h in 1 atm nitrogen flow (ca. 30 ml/min). Under these conditions catalyst crystallization occurs (*23*).

The surface oxides prepared were characterized primarily by X-ray photoelectron spectroscopy because it provides both surface compositional and chemical information. Systematic measurements of photoemission intensities as a function of oxidation temperature and alloy composition were made to obtain thermodynamic and kinetic information about the surface oxidation processes and the resulting oxide structures. XPS spectra were taken with a Kratos-XSAM 800 spectrometer equipped with a DS 300 data processing system. Mg$K\alpha$ radiation was used as the X-ray excitation source. The spectrometer was operated in the fixed analyzer transmission (FAT) mode with a pass energy of 38 eV. The spectral areas determined were corrected for instrumental parameters, photoionization cross sections, and electron mean free paths. The binding energies were corrected by using the C(1*s*) line from the adventitious carbon. The value for the C(1*s*) line from contamination was assumed to be equal to 284.8 eV. Binding energy shifts of the photoelectrons, kinetic energy shifts of the Auger electrons, and changes in the satellite structure of Cu(2*p*) photoelectrons and the Mn(3*p*) multiplet splitting were carefully followed to obtain detailed information on the oxygen interactions of various Cu–Mn alloys during the oxidation experiments.

Catalyst activity tests for CO oxidation were run on 100 mg of ground Cu–Mn(33%) alloy and commercial Hopcalite using a continuous flow reactor monitored by gas chromatography. The Cu–Mn(33%) alloy was activated at 400°C for 1 h in oxygen while the commercial Hopcalite was activated at 250°C for 1 h in oxygen. The higher activation temperature for the alloy sample was chosen as a temperature where both amorphous-like Cu^{2+} and crystalline species were present as indicated by the XPS results. It was hoped that the crystallization process would result in a roughened alloy surface. It can be noted that this temperature of 400°C is still lower than that required to completely crystallize commercial Hopcalites (550°C). After activation, a 12 : 1 O_2-to-CO mixture was reacted over both catalyst systems. The commercial sample was reacted to 25°C and the alloy at 160°C due to the lower surface area of the alloy catalyst.

RESULTS

Oxidation of Cu–Mn Alloys

Area ratios of the Mn(2*p*)-to-Cu(2*p*) lines and Mn surface enrichment factors of Cu–Mn alloys oxidized in 1 atm oxygen as a function of oxidation temperature are shown in Figs. 1 and 2, respectively. For a series of Cu–Mn alloy oxidations, the use of the Cu(2*p*) satellite and Cu(LMM) Auger lines has facilitated the confirmation of Cu_2O and CuO at low and high temperature ranges, respectively. The products of room-temperature oxidation showed Mn enrichment while at intermediate temperatures (100–200°C), the Mn oxide signal was suppressed and the Cu oxide signal increased. This tendency was more pronounced for alloys with higher Cu content.

For high-temperature oxidations (300–500°C), the surface enrichment factors strongly increased for Mn. These findings can be interpreted as an overgrowth of the thermodynamically more stable Mn oxides over Cu oxides within this temperature regime. Interaction of oxygen with alloys of higher Mn content induced a marked segregation of Mn, particularly pronounced as temperature increased. The surface enrichment of Mn in oxides several layers thick was dependent both on the reaction temperature and on the alloy bulk composition; for the higher oxidation temperatures and Mn concentrations, more Mn surface enrichment was observed. For instance, the

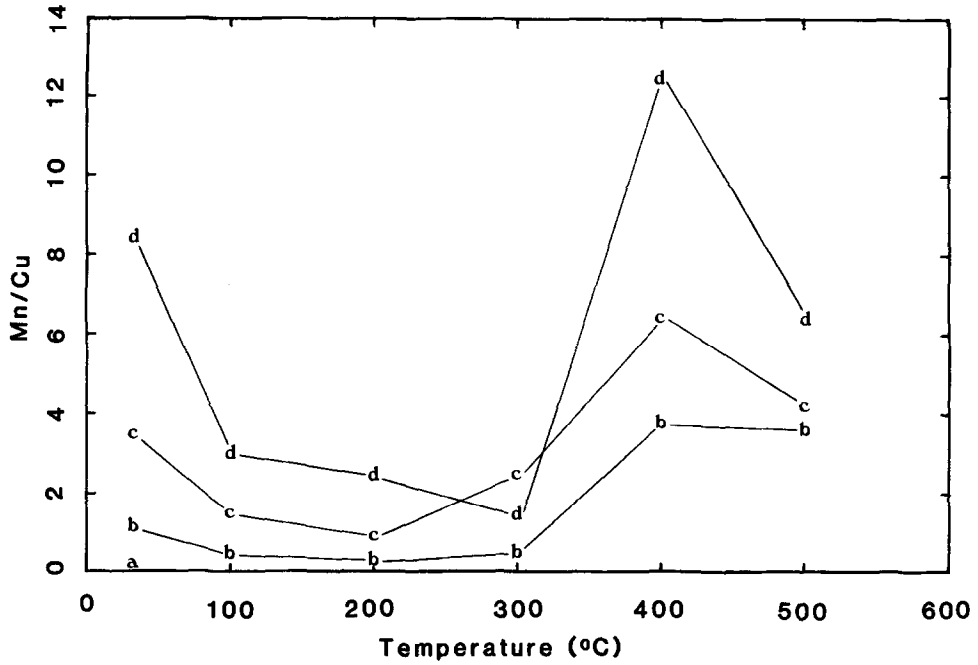

FIG. 1. Area ratios of Mn(2*p*) to Cu(2*p*) as a function of oxidation temperature for surfaces oxidized in 1 atm oxygen with a bulk composition of (a) Cu–Mn(10%), (b) Cu–Mn(33%), (c) Cu–Mn(50%), and (d) Cu–Mn(67%).

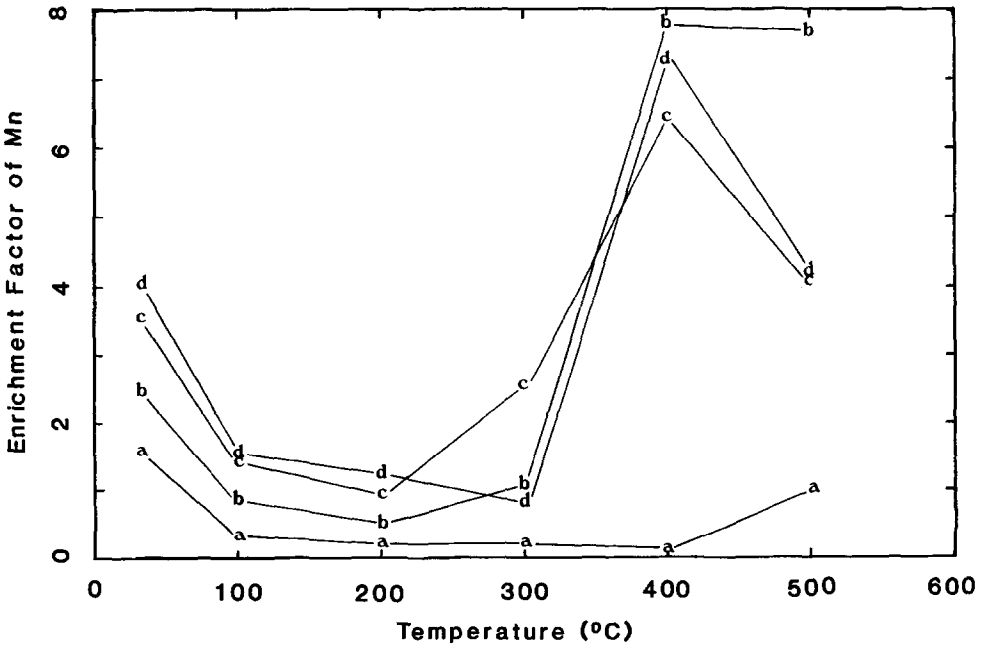

FIG. 2. Surface enrichment factors of Mn as a function of temperature for surfaces oxidized in 1 atm oxygen with bulk compositions of (a) Cu–Mn(10%), (b) Cu–Mn(33%), (c) Cu–Mn(50%), and (d) Cu–Mn(67%).

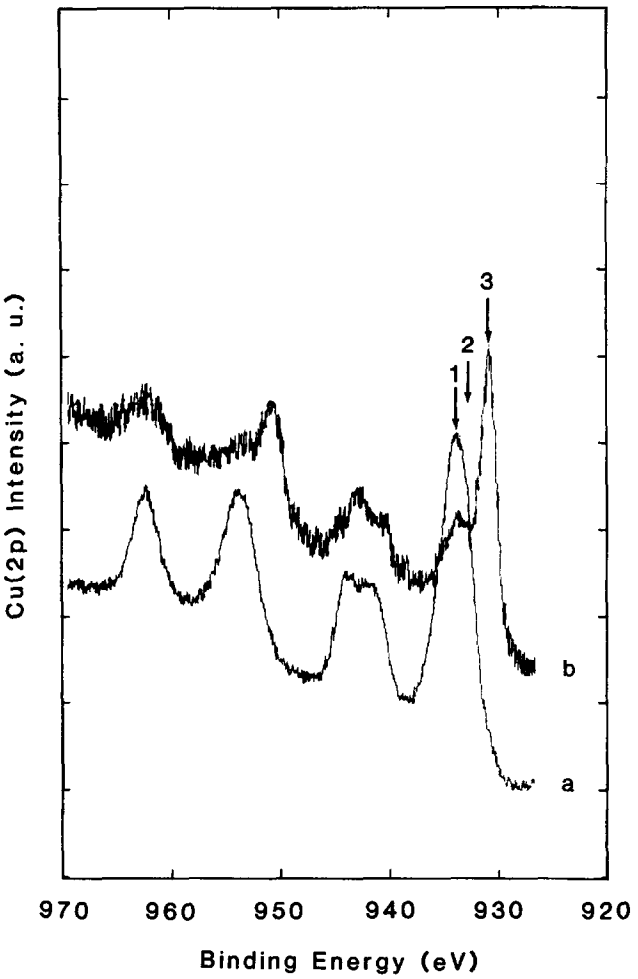

FIG. 3. Spectra of the Cu(2*p*) region of the oxide layer of a Cu–Mn(33%) alloy oxidized for 1 h in 1 atm oxygen at (a) 300°C and (b) 400°C.

high-temperature oxidation of alloys with more than about 66% Mn caused a complete segregation of Mn oxides whereas the alloy with 10% Mn was covered primarily by CuO. Above 400°C, Cu oxide overgrowth causes the Mn-to-Cu ratio to drop.

Interestingly, in the Cu–Mn(33%) alloy, the Mn-to-Cu ratio remains unchanged with temperature. This is a strong indication that a stoichiometric reaction in the oxide overlayer has been established, thus drawing special attention to the Cu–Mn(33%) alloy for preparation of mixed valent oxide overlayers.

Figure 3 shows spectra of the Cu(2*p*) region of a Cu–Mn(33%) alloy oxidized at 300 and 400°C for 1 h in 1 atm oxygen. For the Cu–Mn(33%) and Cu–Mn(50%) alloys, chemically mixed oxide layers were found after oxidation at 400 and 500°C, whereas physically layered structures of oxides were formed after lower-temperature oxidations or for other alloy compositions.

Decomposed spectra of the Cu(2*p*) region of the Cu–Mn(33%) alloy oxidized at 400°C for 1 h in 1 atm oxygen are shown in Fig. 4. The decomposed Cu(2*p*) spectra indicate that the surface oxide in this case is a mixed compound oxide with a spinel structure, as will be discussed in detail.

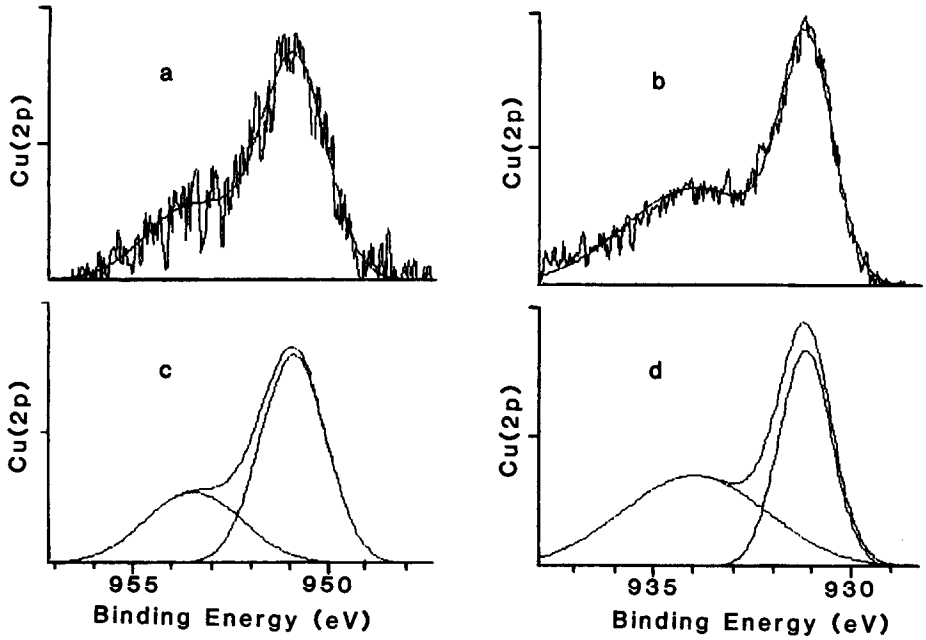

FIG. 4. Decomposed spectra of the Cu(2*p*) region of a Cu–Mn(33%) alloy oxidized at 400°C for 1 h in 1 atm oxygen: (upper) comparison of raw and best-fit peaks and (lower) comparison of best-fit and decomposed peaks.

Commercial Hopcalite

Representative spectra of the Cu(2*p*) region for commercial Hopcalite are shown in Fig. 5. The commercial Hopcalite was activated at 220°C for 2 h in 1 atm oxygen flow (ca. 30 ml/min) (Fig. 5a) and then deactivated at 550°C for 10 h in 1 atm nitrogen flow (ca. 30 ml/min) (Fig. 5b). In Fig. 6, the Cu(2*p*) region of a model Hopcalite, Cu–Mn(33%), is compared with that of crystallized commercial Hopcalite. The binding energies and peak shapes in the Cu(2*p*) region of the Cu–Mn(33%) alloy oxidized at 400°C (Fig. 3b) resemble those of the crystallized commercial Hopcalite (Fig. 5b). Moreover, the planar model catalyst prepared in this study is very similar to bulk $CuMn_2O_4$ prepared by Broemme and Brabers (*25*). Most convincing is a comparison of Fig. 3 of the model Hopcalite and Fig. 5 of the commercial Hopcalite. Similar oxidation states are present before and after crystallization for both types of samples. In addition, the 300°C spectra of both samples appear to be of an amorphous material based on the broad Cu(2*p*) peaks. After crystallization a better spinel structure results for the planar model than for the commercial Hopcalite.

Catalytic Activity Test of Planar Model Catalysts

The preliminary activity tests were run to demonstrate the catalytic nature of the planar model catalyst. This is currently being studied in more detail (*26*). CO conversion is plotted against reaction time for model and commercial catalysts in Fig. 7. The model catalyst behaves in a manner similar to that of the commercial catalyst. For the model catalyst, CO conversion is lower and the reaction is run at a higher temperature than the commercial catalyst due to the very low surface area of the model catalyst (0.01 m^2/g). On the basis of the rough assumption that the activity doubles with every 10°C rise in reaction temperature and considering surface areas of the catalysts, the activity of the model catalyst has ap-

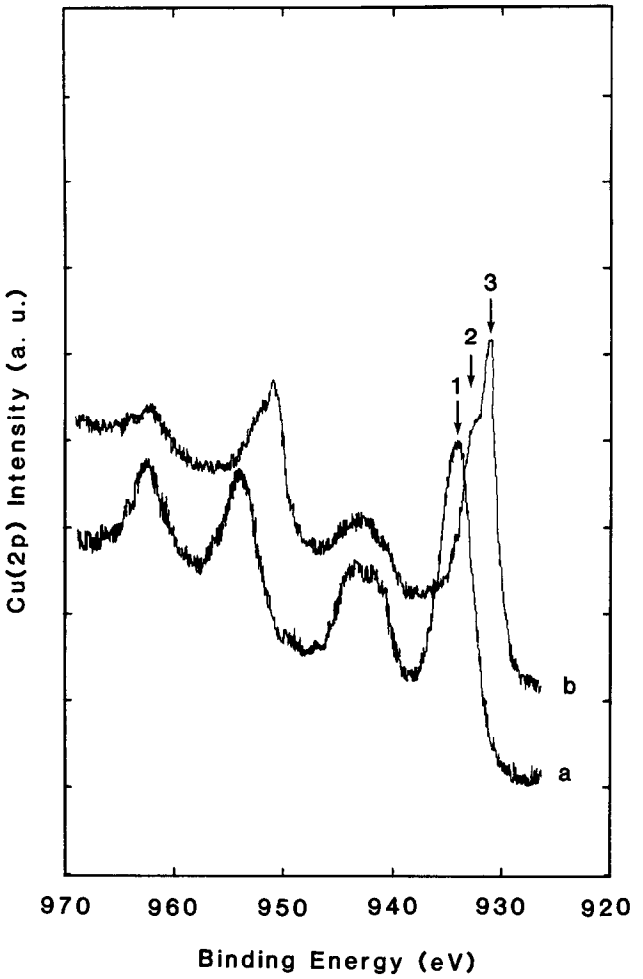

FIG. 5. Spectra of the Cu(2*p*) region of commercial Hopcalite: (a) activated at 220°C for 2 h in 1 atm oxygen flow (ca. 30 ml/min) and (b) deactivated at 550°C for 10 h in 1 atm nitrogen flow (ca. 30 ml/min).

proximately the same activity as the commercial catalyst.

DISCUSSION

Preparation of Planar Model Catalysts

From a careful consideration of the stability of the spinel structure in the phase diagram Cu–Mn–O (*25*), the stoichiometric $CuMn_2O_4$ phase is expected to be stable in the region of 700 to 900°C. Above that region the compound seems to disintegrate into a Mn-rich spinel and CuO; below that region a Cu-rich spinel is obtained in the presence of Mn_2O_3. It has also been reported that it is impossible to prepare stoichiometric $CuMn_2O_4$, which is cubic at room temperature, and that the cubic spinel can be prepared only with excess Cu for $Cu_{1+x}Mn_{2-x}O_4$ (*27*). The preparation method of a thin surface spinel film, however, will be quite different from that of the bulk spinel since it is complicated by thermodynamic and kinetic phenomena which occur in the surface zone. These complicating phenomena are associated with surface segregation, oxygen adsorption and desorption, oxygen bulk penetration, and oxidation and oxide displacement reactions as observed in our previous studies (*24*). Therefore, to accomplish the objective of

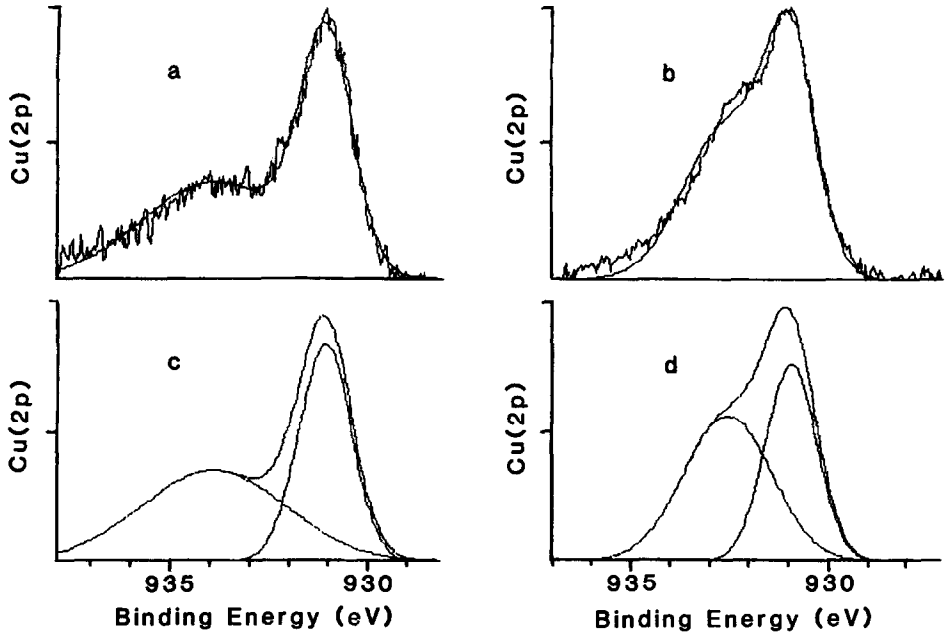

FIG. 6. Comparison of the Cu(2*p*) region of Hopcalites: (a) a model Hopcalite prepared in this study by oxidation of a Cu–Mn(33%) alloy at 400°C for 1 h in 1 atm oxygen, comparison of raw and best-fit peaks; (b) a commercial Hopcalite crystallized at 550°C for 10 h in 1 atm nitrogen flow (ca. 30 ml/min), comparison of raw and best-fit peaks; (c) comparison of best-fit and decomposed peaks; (d) a commercial Hopcalite as in (b), comparison of best-fit and decomposed peaks.

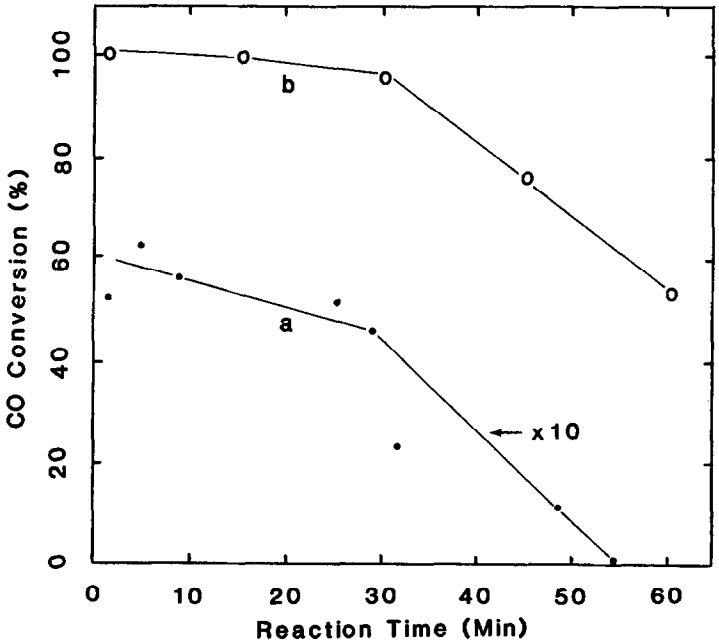

FIG. 7. Plot of CO conversion against reaction time for (a) a model catalyst prepared by Cu–Mn(33%) oxidation run at 160°C and (b) a commercial catalyst run at room temperature.

preparing a planar model for Hopcalite, these solid state phenomena must be fully understood. On the basis of this background, oxidation should be carried out under both kinetic and thermodynamic control, in terms of alloy composition, oxygen activity, and oxidation temperature and time. In this respect, the preceding oxidation studies on Cu, Mn, and Cu–Mn alloys (*24*) provide a wealth of information and the key needed to produce a planar model of Hopcalite.

The goal of this portion of the research was to produce a stoichiometric composition, similar to that of Hopcalite, on the surface of Cu–Mn alloys. This process within the several topmost surface layers will be controlled by bulk composition, surface segregation, stabilities of Cu and Mn oxides, and relative reaction rates of oxide formation. In particular, three parameters should be taken into account to prepare a surface mixed oxide: (i) concentration of oxides in the surface region, (ii) diffusion rates of oxides and (iii) solubility and reactivity of oxides. It is known that the Cu oxides and Mn oxides have good solubility. Bulk mixed oxides can form according to information provided from the equilibrium diagram (*28, 29*). For alloys with 10% Mn, the surface consists primarily of Cu oxides, which is more pronounced at medium-temperature oxidation due to the slower diffusion of Mn to the surface region than Cu (Figs. 1 and 2). On the other hand, for alloys with 66 and 81% Mn, the surface consists mainly of Mn oxides. This is especially pronounced in high-temperature oxidation due to the faster diffusion of Mn to the surface region. For alloys with intermediate composition, Cu–Mn(33%) and Cu–Mn(50%), the surface mixed oxide could be prepared by oxidation under the appropriate reaction conditions in terms of oxidation temperature and oxygen activity. The temperature and oxygen activity required had to be high enough to overcome the difference in the free energy of oxide formation for Cu oxides and Mn oxides to ensure that Cu oxides could form. For the other bulk compositions, only separated, layered mixtures of oxides, or almost solely Cu oxides or Mn oxides could be prepared because the composition of the surface region was far from that needed for stoichiometric $CuMn_2O_4$ formation.

Even if the concentration requirement is satisfied during surface oxidation, the diffusion of the cations in the oxide layer must be fast enough to provide an interdiffusional reaction and to produce the surface mixed oxide. At low temperatures, less than about 300°C for the oxidation of the Cu–Mn(33%) and Cu–Mn(50%) alloys, the second requirement was not satisfied so that only physical mixtures of oxides, or mainly Cu or Mn oxides, were observed.

For comparison, note studies of oxygen interaction with Ni–Fe(24%) (100) surface by Brundle *et al.* (*30*). They showed that at 2.7 monolayers of oxygen, the surface Fe concentration was nearly three times the original and the alloy surface was entirely oxidized at room temperature. More relevant to this study are the oxidation studies of Ni–Fe alloys at 500°C by Wandelt and Ertl (*31*). They showed that oxidation of alloys with less than about 70% Ni caused a complete segregation of Fe_2O_3, whereas for alloys containing more than 70% Ni a mixed oxide layer was probably formed. The final passivation layer contained Ni(II) and Fe(III) and/or Fe(II) ions. They speculated that nickel ferrite had formed as a spinel structure. Experimental evidence for the latter is, however, weak.

Characterization of Planar Model Catalysts

One of the major problems in the crystal chemistry of mixed oxide spinels is the determination of the valencies and distribution of the cations among the tetrahedral and octahedral sublattice sites of the spinel structure. This can be particularly problematic if two different metals are present, each of which can adopt more than one valence state. Such is the case for $CuMn_2O_4$, where

both Cu and Mn exist in more than one chemical state and in different configurational sites.

Since heterogeneous catalysis occurs on the very outer surface of solids, previous activity studies (*17*) correlated with bulk composition and structural changes are doubtful. This is particularly true where commercial samples have been examined (*15*). The nature of surface phases of Hopcalite has not been examined closely (*23*). XPS is a well-established surface characterization tool of catalysts. However, XPS has not been used extensively in the past to study the catalytically important parameters of Hopcalite. In the present study, XPS was used to examine changes in the surface composition and oxidation states of Cu and Mn as they were affected by a variety of heat treatments in oxygen environments. The experimental proof for the formation of a mixed compound oxide on the surface will be discussed here. XPS can be used directly to determine the valence distribution in mixed oxides. Since core levels of atoms may shift due to valence changes and different crystallographic sites, the splitting or shifting of core levels is a direct proof of the presence of nonequivalent cations (*32*).

The binding energies for O, Cu, and Mn are summarized in Table 2. The Cu(2*p*) peaks after oxidation of Cu–Mn(33%) for 1 h at 300°C (Fig. 3a) are compared with those of oxidation at 400°C (Fig. 3b). The decomposed Cu(2*p*) peaks of the Cu–Mn(33%) surface oxidized at 400°C for 1 h are shown in Fig. 4. The binding energies for O(1*s*) were typical for chemisorbed oxygen at 531.9 eV and lattice oxygen at 530.0 eV. Cu(LMM) Auger signals were similar to those from Cu(II) in kinetic energy and peak shape.

Drastic changes in the spectra were observed in the Cu(2*p*) region. The significant features in this spectral region are the spin–orbit split $2p_{1/2}$ and $2p_{3/2}$ peaks along with the shake-up satellite peaks. The Cu species of the Cu–Mn(33%) surface oxidized at 300°C for 1 h consists primarily of Cu(II) as indicated by the existence of strong satellite structure (Fig. 3a). After oxidation at 400°C for 1 h, differences in the position of the satellite peaks with respect to their core level peaks and in the binding energy of the core level $2p_{1/2}$ and $2p_{3/2}$ peaks are observed (Fig. 3b). The Cu–Mn(33%) oxidized at 400°C for 1 h shows the appearance of a new peak at an unusually low binding energy, as well as a decrease in the Cu(II) concentration in the surface region. This is similar to the spectrum of the commercial Hopcalite catalyst in the Cu(I)/Mn(IV) form (Fig. 5b). Here the new Cu($2p_{3/2}$) binding energy is 931.1 eV—an unusually large negative shift relative to metallic Cu. After the 400°C oxidation, the binding energies are shifted 2.8 eV to lower values. This binding energy is 1.7 eV lower than that generally observed for metallic Cu or Cu_2O. Also, this binding energy is similar to those seen by D'Huysser *et al.* (*33, 34*), Haber (*35*), Broemme and Brabers (*25*), and, more recently, Cocke and Veprek (*36*).

Such negative chemical shifts of the signals, with respect to those of clean Cu metal, have been explained in ferrites and chromites in octahedral symmetry by D'Huysser *et al.* (*33, 34*) and in molybdates by Haber *et al.* (*35*). Generally, the chemical shift is primarily due to the initial charge

TABLE 2

Binding Energies of the Principal XPS Lines Observed in Planar Model Catalysts

Lines	Oxidation state	Binding energy	FWHM
Cu($2p_{1/2}$)	0	932.8	
	1	931.1 (931.1)[a]	1.6
	2	933.9 (935.1)	4.3
Cu($2p_{2/3}$)	0	952.6	
	1	950.9 (950.8)	1.9
	2	953.5 (954.8)	2.9
Cu(LMM)	?	335.8[b]	2.6
Mn($2p_{1/2}$)	3	(642.6)	
	4	(641.6)	
	?	642.0	4.5
O(1*s*)	Chemisorbed	531.9	2.6
	lattice	530.0	1.6

[a] Values in parentheses are from Veprek *et al.* (*23*) and Broemme and Brabers (*25*) for comparison.
[b] Derived from its kinetic energy.

state, Madelung potential, and final state relaxation energy. These latter authors have attributed the negative binding energy shift with respect to metallic Cu to the difference in the Madelung potentials.

According to studies by Broemme and Brabers (*25*), the Cu($2p_{3/2}$) peak of tetrahedral Cu(I) shows a chemical shift of about 2 eV compared with those in Cu_2O (930.7 eV) whereas the Cu($2p_{3/2}$) peak of octahedral Cu(II) shows the same chemical shift as those in CuO (933.6 eV). This is in excellent agreement with this study.

The latest and most thorough Hopcalite catalyst study by Veprek *et al.* (*23*) has found that the Cu($2p_{3/2}$) peak after deactivation at 550°C in nitrogen, presumed a spinel Cu(I), shows a chemical shift to a lower binding energy of about 1.7 eV than those in Cu_2O (931.1 eV). In contrast, the Cu($2p_{3/2}$) peak after activation in oxygen at 220°C, presumed an amorphous Cu(II), shows a chemical shift to higher binding energy of about 1.3 eV than those in CuO (935.1 eV). All the comparisons made above suggest that the Cu–Mn(33%) surface oxidized at 400°C consisted primarily of Cu(I) in the tetrahedral symmetry of a spinel with less Cu(II). Additional evidence for certain Cu valencies can be obtained by checking for the presence and relative intensities of satellite peaks. The satellite peaks in the Cu($2p$) region of Cu–Mn(33%) surface oxidized at 400°C were 12 eV away from the main peaks whereas typical satellite shifts in Cu(II) are 6–10 eV, and hence, the presence of Cu(I) is confirmed.

To ascertain the oxidation state of Cu cations in the surface oxides prepared, the broadening of the core level peaks can be analyzed by comparison with the spectra of compounds containing known species of ions. Peak broadening of the core levels with the presence of mixed oxidation states is expected compared to pure Cu and Mn. The full widths at half-maximums of Cu($3p$) and Mn($3p$) of the Cu–Mn(33%) surface oxidized at 400°C were broader than those of pure Cu and Mn oxidized under similar conditions, with Cu($3p$) being more pronounced. This seems to support mixed oxidation states of Cu and Mn in the spinel structure.

The core levels of Mn($2p$) also support the proposed model. In general, the binding energy of core levels shifts ca. 1 eV with a one unit change in the ionic charge of an atom, under the assumption that no other effects (such as covalency) interfere. In this case, covalency effects will have only minor influence since the ligands are oxygen ions for both lattice sites. Unfortunately, when mixed Mn oxides exist on the surface, the Mn($2p$) peaks are broad in nature and the shifts in the Mn($2p$) electron binding energies are within the instrumental resolution. This problem was exemplified by Oku *et al.* (*37*) for Mn(II) and Mn(III) states in Mn_3O_4, and site differences for Mn(III) in γ-Mn_2O_3. Thus, the oxidation state of Mn determined from the chemical shifts in this work cannot be confidently assigned. They can, however, be interpreted indirectly by considering other results. A comparison of the Mn($2p$) values with those for Hopcalite (Table 2) provides an indication that Mn may be present as Mn(III) and Mn(IV) ions since the Mn($2p$) binding energy (642.0 eV) is between Mn(III) (642.6 eV) and Mn(IV) (641.6 eV). Mn(IV) with $3d^3$ electronic configuration is probably in octahedral symmetry as predicted (*26*, *38*). On those occasions when Cu(I) has been observed, Mn(IV) has also been present (*23*, *36*). Note that mainly Mn(IV) ions were found to be present after deactivation of Hopcalite whereas this study seems to show a mixture of Mn(IV) and Mn(III).

The multiplet splitting has been previously used to examine the oxidation states of Mn in Mn spinels (*23*, *36*). Shirley (*39*) has shown that the experimental values for Mn($3s$) multiple splitting in $3d$ transition metal compounds depend on the number of $3d$ electrons, being maximal at ca. 7 eV for $3d^5$ ions and decreasing ca. 1 eV per electron if the number of electrons is changed. The multiplet splittings reported by Shir-

ley for Mn(II)($3d^5$), Mn(III)($3d^4$), and Mn (IV)($3d^3$) are in good agreement with our results. It is seen that the Mn(3*s*) has somewhat broader peaks as one would expect from the range of coordination found in the mixture of Mn(III) and Mn(IV) ions. The multiplet splitting position may be indicative of Mn(IV) with some smaller contribution from Mn(III). However, Mn(3*s*) multiplet splitting could not be fully used since the Mn(3*s*) main peak overlapped with Cu(3*p*) peak. In addition, the low Mn(3*s*) intensity made measurements on the Mn(3*s*) multiplet splitting difficult.

The thickness of the surface oxide can be qualitatively described by comparing the 2*p* and 3*p* Cu-to-Mn peak area ratios. The surface sensitivity of a photoelectron line depends on its kinetic energy, and hence, the 2*p* photoelectron is more surface sensitive than the 3*p* photoelectron. For the Cu–Mn(33%) surface oxidized at 400°C, the Mn(2*p*)-to-Cu(2*p*) area ratio (3.82) was smaller than that of Mn(3*p*) to Cu(3*p*) (4.47). Noting that for a homogeneous bulk $CuMn_2O_4$, the ratio should be two, this suggests that the surface oxide is very thin in terms of photoelectron escape depth and that a Mn-rich oxide phase is below the very thin surface mixed oxide film.

For the Cu–Mn(33%) surface oxidized at 400°C, the oxide surface region is dominated by Cu(I). In the Hopcalite studies by Veprek *et al.* (*23*) they assigned Cu($2p_{3/2}$) at 931.1 eV to Cu(I) in an octahedral environment for the deactivated sample. Note that only Cu(I) ion was found to be present after deactivation of Hopcalite whereas this study shows Cu(I) and some Cu(II) in the surface mixed oxide. Generally, the same results as above were found in the Cu–Mn(33%) and Cu–Mn(50%) alloy surfaces oxidized at 400 and 500°C for 1 h. Under other conditions in terms of oxidation temperature and alloy composition, only physical mixtures of Cu and Mn oxides were obtained primarily due to the complicated factors of the surface reaction, i.e., surface segregation, stabilities of oxides, and differences in diffusion rates. The area ratios of Mn(2*p*) to Cu(2*p*), as well as Cu(I) to Cu(II), depend significantly on the oxidation temperature and alloy composition (Fig. 1). Based on these ratios, the best planar model Hopcalite was obtained when oxidizing the Cu–Mn(33%) alloy at 400°C in 1 atm oxygen. Further studies are required to attain better control of the preparation of the surface mixed oxides and to understand the mechanism involved in this type of solid state reaction.

Comparison of the Planar Models with Commercial Hopcalite

A marked effect from the heat treatments on a commercial Hopcalite was found in the Cu(2*p*) region (Fig. 5). The activated Hopcalite consists primarily of Cu(II) (peak 1) and there is no peak 2 or 3 (Fig. 5a). On the other hand, the deactivated Hopcalite consists mainly of Cu(I) (peak 3) and a shoulder (peak 2) appears at ca. 932.8 eV (Fig. 5b). Comparing Figs. 3 and 5, the spectrum of a surface oxide prepared at 300°C oxidation (Fig. 3a) is very similar to that of the activated commercial Hopcalite (Fig. 5a). Similarly, the spectrum of a surface mixed oxide prepared by 400°C oxidation (Fig. 3b) resembles that of the deactivated commercial Hopcalite (Fig. 5b).

It can be seen that the Cu(2*p*) chemical states are complex. This complexity is due in part to the added presence of Cu(II) (peak 1). Also, the Cu(2*p*) level of tetrahedral Cu(I) (peak 3) shows chemical shifts of ca. 2 eV compared with those in metallic Cu or Cu_2O (peak 2). A difference in Cu cation distributions, as judged from the binding energies and relative intensities of the Cu(2*p*) region (Fig. 6), is observed. Two decomposed peaks (Fig. 6d) are closer to each other than those in Fig. 6c. The Cu(2*p*) binding energy data of the planar model catalysts prepared in this study are in excellent agreement with that of Broemme and Brabers (*25*). It can be seen that the planar model catalysts are similar to the bulk Cu–Mn oxides prepared by them. It ap-

pears that the cation distributions in Cu–Mn oxide spinels are sensitive to heat treatments. They observed that the tetrahedral Cu(I) ions indeed interfere with the electrical transport properties at higher temperatures. This implies that the Cu–Mn redox couples may play an important role in oxidation catalysis of Hopcalite.

CONCLUSIONS

A planar model of Hopcalite has been prepared for the first time by oxidation of Cu–Mn alloys (30–50% Mn) at high temperatures (400–500°C) in 1 atm oxygen. It was established by XPS that for the Cu–Mn(33%) surface oxidized at 400°C, the surface region is dominated by Cu(I) in a tetrahedral environment and Mn(IV) perhaps in an octahedral environment with lesser amounts of Cu(II) and Mn(III). The limited oxidation conditions where the mixed oxides were prepared can be explained by thermodynamic and kinetic reasoning. The CO oxidation reaction has been used to show the catalytic similarity of the planar model to the commercial Hopcalite. This will allow future studies on the mechanism of oxidation catalysts of this system to be correlated with activity.

The charge transfer resonance, which appears to be invaluable in oxidation catalysis of Hopcalite using this new planar model, is now open for further investigation. Two questions that need to be addressed in future research are (i) what is responsible for Hopcalite deactivation at high temperature and (ii) what plays the most important role in Hopcalite catalysis: a charge transfer resonance, phase change, or surface segregation?

ACKNOWLEDGMENTS

D. Eric Halverson, manager of the Texas A&M University Surface Science Center, provided valuable assistance in obtaining the XPS spectra. This work was funded primarily by the Interior Department's Bureau of Mines under Contract J0134035 through Department of Energy Contract DE-AC07-761D01570. The authors also acknowledge with thanks the partial financial support of this project by the Board of Regents of Texas A&M University, the Texas Advanced Technology Research Program, and the Robert A. Welch Foundation.

REFERENCES

1. Cocke, D. L., Johnson, E. D., and Merril, R. P., *Catal. Rev. Sci. Eng.* **26,** 163 (1984).
2. Thomas, J. M., and Lambert, R. M., "Characterization of Catalysts," Wiley, New York, 1980.
3. Renou, A., *J. Catal.* **78,** 77 (1982).
4. Haller, G. T., *Catal. Rev. Sci. Eng.* **23,** 474 (1981).
5. Poling, G. W., *J. Colloid Interface Sci.* **34,** 365 (1970).
6. Pritchard, J. W., and Chatterick, T., *in* "Experimental Methods in Catalytic Research" (R. B. Andersson and P. T. Dawson, Eds.), Vol. III. Academic Press, New York, 1976.
7. Greenler, R. G., *J. Chem. Phys.* **44,** 310 (1966).
8. Jones, H. A., and Taylor, H. S., *J. Phys. Chem.* **27,** 623 (1923).
9. Stone, F. S., "Advances in Catalysis" (D. D. Eley, P. W. Selwood, and P. B. Weisz, Eds.), Vol. 13, p. 1. Academic Press, San Diego, 1962.
10. Lamb, A. B., Bray, W. C., and Frazer, J. C. W., *Ind. Eng. Chem.* **12,** 213 (1920).
11. Dermott, J. M. C., *in* "Pollution Control Review," Vol. 2, Noyes Data Corp., Park Ridge, IL, 1971.
12. Lawrence, A. A., *in* "Pollution Control Review," Vol. 8, Noyes Data Corp., Park Ridge, IL, 1972.
13. Margolis, L. Y., *Catal. Rev. Sci. Eng.* **8,** 241 (1973).
14. Jagow, R. B., Katan, T., Lamparter, R. A., and Ray, C. D., American Society of Mechanical Engineers Technical Report 77-ENAS-28.
15. Dondur, V., Lampa, S., and Vucelic, D., *in* "Proc. 4th Int. Symp. Heterogeneous Catalysis, Part 2," p. 151. 1979.
16. Dondur, V., Lampa, S., and Vucelic, D., *in* "Proc. 2nd Europ. Symp. Thermal Anal." (D. Dollimore, Ed.), p. 182. Haydon, London, 1981.
17. Kanungo, S. B., *J. Catal.* **58,** 419 (1979).
18. Schwab, G. M., and Kanungo, S. B., *Z. Phys. Chem. N. F.* **107,** 109 (1977).
19. Sinha, A. P. B., Sanjana, N. R., and Biswas, A. B., *J. Phys. Chem.* **62,** 191 (1958).
20. Jogalekar, P. P., and Sinha, A. P. B., *Indian J. Pure Appl. Phys.* **5,** 9 (1967).
21. Padalia, B. D., Krishnan, V., Patni, M. J., Radhakrishran, N. K., and Gupta, S. N., *J. Phys. Chem. Solids* **34,** 1173 (1973).
22. Dowden, D. A., *in* "Surface Science," Vol. II, International Atomic Energy Agency, Vienna, 1975.
23. Veprek, S., Cocke, D. L., Kehl, S., and Oswald, H. R., *J. Catal.* **100,** 250 (1986).

24. Yoon, C., and Cocke, D. L., *Appl. Surf. Sci.* **31,** 118 (1988).
25. Broemme, A. D. D., and Brabers, V. A. M., *Solid State Ionics* **16,** 171 (1985).
26. Cocke, D. L., Yoon, C., Puckhaber, L. S., and Cheung, H., in press.
27. Vanderberghe, R. E., *Phys. Stat. Sol.* **50,** K85 (1978).
28. Vanderberghe, R. E., Robbrecht, G. G., and Brabers, V. A. M., *Mater. Res. Bull.* **8,** 571 (1973).
29. Driessens, F. C. M., and Rieck, G. D., *Z. Anorg. Allg. Chem.* **351,** 48 (1967).
30. Brundle, C. R., Silverman, E., and Madix, R. J., *J. Vac. Sci. Technol.* **16,** 474 (1979).
31. Wandelt, K., and Ertl, G., *Surf. Sci.* **55,** 403 (1976).
32. Oku, M., and Hirokawa, K., *J. Solid State Chem.* **30,** 45 (1979).
33. D'Huysser, A., Lerebours-Hannoyer, B., Lenglet, M., and Bonnelle, J. P., *J. Solid State Chem.* **39,** 246 (1981).
34. D'Huysser, A., Luchetti, A., Wrobel, G., and Bonnelle, J. P., *J. Microsc. Spectrosc. Electron* **2,** 609 (1977).
35. Haber, J., Machej, T., Ungier, L., and Ziolkowski, J., *J. Solid State Chem.* **25,** 207 (1978).
36. Cocke, D. L., and Veprek, S., *Solid State Commun.* **57,** 745 (1986).
37. Oku, M., Hirokawa, K., and Ikeda, S., *J. Electron Spectrosc. Relat. Phenom.* **7,** 465 (1975).
38. Radhakrishnan, N. K., and Biswas, A. B., *Phys. Stat. Sol.* **44,** 45 (1977).
39. Shirley, D. A., *Phys. Scr.* **11,** 117 (1975).